International Journal of
Physical Sciences

ABOUT IJPS

The International Journal of Physical Sciences (IJPS) is published twice monthly (one volume per year) by Academic Journals.

International Journal of Physical Sciences (IJPS) is an open access journal that publishes high-quality solicited and unsolicited articles, in English, in all Physics and chemistry including artificial intelligence, neural processing, nuclear and particle physics, geophysics, physics in medicine and biology, plasma physics, semiconductor science and technology, wireless and optical communications, materials science, energy and fuels, environmental science and technology, combinatorial chemistry, natural products, molecular therapeutics, geochemistry, cement and concrete research, metallurgy, crystallography and computer-aided materials design. All articles published in IJPS are peer-reviewed.

Contact Us

Editors

International Journal of Physical Sciences

Table of Contents: Volume 13   Number 11,   16 June, 2018

<u>ARTICLE</u>

AJ ACADEMIC JOURNALS
expand your knowledge

International Journal of Physical Sciences

Full Length Research Paper

Gross alpha and beta activity concentrations in soil and some selected Nigerian food crops

Chijioke M. Amakom*, Chikwendu E. Orji, Benedict C. Eke, Chinedu Iroegbu and Bridget A. Ojakominor

Radiation and Health Physics Research Group, Department of Physics, Federal University of Technology, Owerri, Imo State, Nigeria.

Gross alpha and beta activity concentrations in soil, cassava and fluted pumpkin (leaf and stem) were investigated using a gas flow proportional counter. The gross alpha activity concentrations for the fluted pumpkin were between 3.55 and 13.95 Bq/Kg and 3.53 and 3.61 Bq/Kg for the leaves and stems, respectively. The gross alpha activity concentrations for cassava and soil samples ranged from 0.07 to 0.60 Bq/Kg and 0.35 to 0.53 Bq/Kg, respectively while the gross beta activity concentrations ranged from 0.43 to 0.89 Bq/Kg and 0.46 to 1.04 Bq/Kg for the cassava and soil samples, respectively. The gross alpha and beta activity concentrations in cassava, fluted pumpkin and soils samples have been determined using alpha/beta spectroscopy. The result of thestudy showed that the Iva-valley coal mine area has lower gross alpha and beta activity concentrations compared to other areas of the country. This shows that the coal mining activities in the area may not have increased the radiation burden of the area.

Key words: Gross, alpha, beta, concentration, activity, food, crop.

INTRODUCTION

Geographical location upon the earth surface influences the level of terrestrial radiation as a result of the radionuclides concentration in soil which largely depend on the local geology (Farai and Jibiri, 2000; Jibiri and Bankole, 2006). So, as plant uptake of radionuclides varies from species to species and also from place to place, the intake of different food products forms a secondary source of exposure to radionuclides (Addo et al., 2013).

The quality of foodstuffs produced is to a large extent dependent on the nutritional status of the soil on which they are grown (Jibiri, 2001), likewise the distribution of radionuclides in the different segments of a plant is dependent on the chemical characteristics and several other parameters contributing to the soil-plant interactions (Shanthi et al.,2009).

There are two mechanisms for the contamination of vegetation, that is, by root uptake or directly by aerial

*Corresponding author. E-mail: camakom@gmail.com.

deposition of fallout radionuclides on plants. It is necessary to carry out an accurate assessment of these radionuclides in the daily used food materials in order to ascertain the degree of risk and deleterious effects to the public health. Fluted pumpkin and cassava are food sources largely consumed daily in Nigeria, this make them potential radioactive contamination pathway for the local population. Fluted pumpkin which is a leafy vegetable is found in most delicacies consumed in Nigeria, whereas cassava (a tuber) constitutes one of the major food sources for carbohydrates. The analysis of these radionuclides in soil and food stuffs is an important part of the environmental monitoring program. These natural radioactive sources are the largest contributor of the radiation dose received by mankind. This researched is aimed at estimating the level of radionuclide concentrations found in these staple food sources.

MATERIALS AND METHODS

Study area

The study area is the old coal mining area of Enugu Urban area, located approximately at Latitude 060 301°N and Longitude 070 301°E in the Southern part of Nigeria. The study area is bounded in the Iva Valley Coal Mine Settlement area of Enugu, South- Eastern Nigeria, Located within the Coordinates of 6°27'0"N and 7°27'0"E. The area is famous for its coal mining activities (Amakom et al., 2015). There are road network that connects or link to each of the urban areas in the state.

Sample collection

The cassava and fluted pumpkin (leaf and stem) samples were collected in four different farms within the old coal mine area.

Four different samples of cassava specimens were collected from the selected farms while fluted pumpkins were collected in two farms along the bank of the Ekulu River that snakes from the Iva-valley into the main urban areas of Enugu. At the point of collection of the individual cassava and fluted pumpkin samples, soil samples were also collected at a depth of 10 cm, which is assumed to be the rooting zone of the plants. About 1 kg of soil samples were collected at each sample point using a hand trowel and black polythene bags. All the collected samples were labeled accordingly and transported to the laboratory for further analysis.

Sample preparation

The crops (fluted pumpkin and cassava) were thoroughly washed with tap water and then rinsed with distilled water to remove surface sand and other forms of contamination. In the laboratory, the cuticles of the cassava were removed with a stainless steel knife (previously rinsed with distilled water) and the edible parts were cut into pieces of about 10 mm^2 and put together in polyethylene materials for refrigeration. The samples were freeze-dried for three days after which they were grinded by means of a cleaned industrial blender and kept separately in their respective containers (which were previously washed and rinsed with distilled water and dried). The samples were then oven dried at a constant temperature of 100°C until a constant mass was achieved.

For the fluted pumpkin, the leaf was separated from the stem and both the leaf and stem were sun-dried for three days, and then oven dried at a temperature of 100°C until a constant weight was attained. The soil samples were also sun-dried for 3 days, after which they were oven dried to attain a constant mass.

Each sample was further crushed and sieved using a 60 μm mesh sieve to obtain smaller grain-sized particle. The individual samples were weighted and sealed-packed in 500 ml plastic containers and was ready for alpha/beta spectroscopy.

Instrumentation

The equipment used for the gross alpha and gross beta counting is a gas flow proportional counter with 450 mg/cm^3 thick window of diameter 0.06 m. It is a EURISYS MEASURE IN20 low background multiple (eight) channel alpha and beta counter. The counting system incorporates an anti-coincident guard counter used to eliminate interference from high-energy cosmic radiation into the measuring environment. The chambers are covered with 0.1 m lead and the inside dimensions are 0.48 × 0.28 × 0.10 m^3 with stainless steel linings to prevent part of ambient gamma rays from entering the measuring environment. Thus the only contribution to the counting would be from impurities in the chamber constructing materials. The counting gas is an argon-methane mixture in the ratio of 90 to 10%. For signal processing purpose, the system is connected to a microprocessor IN – SYST, a spreadsheet programme, QUARTTRO – PRO and a graphic programme MULTIPLAN (Akpa et al., 2004).

The beta and alpha specific activities were calculated using the following expression (Jibiri and Fasae, 2012):

$$\text{Specific activity } (\alpha, \beta) = \frac{C.R\,(\alpha,\beta) - B.C.R(\alpha,\beta)}{S.E \times C.E \times W} \tag{1}$$

Where C.R is the counting rate, B.C.R is the background counting rate, S.E is sample efficiency, C. E is channel efficiency and W is weight of sample.

The detector background measurement is aimed at getting the channel efficiency. It was carried out with empty counting planchette, washed with deionized water and dried. The operational high voltages, 1600 V for alpha and 1700 V for beta was set and background radioactivity was measured for thirteen cycles for 900s per cycle for alpha background and twenty-five cycles of 180s per cycle for beta. A histogram and a scatter graph of the counts against channel number were obtained for all the eight channels measured simultaneously. The background count rates were recorded in counts per minute in alpha only and beta only modes.

RESULTS AND DISCUSSION

The results of the gross alpha and beta activity concentrations in the Fluted pumpkin (*Ugu*) leaf, stem and their constituent soils are presented in Table 1. The alpha activity concentrations for the Ugu leaf were 3.55 ± 2.05 and 13.95 ± 4.03 Bq/Kg for the locations 1 and 2 respectively while their corresponding beta activity concentrations were 80.32 ± 2.25 and 12.67 ± 1.82 Bq/Kg. The gross alpha activity concentrations for the Ugu stems were 3.61 ± 2.08 and 3.53 ± 2.04 Bq/Kg for the locations 1 and 2 respectively with a corresponding gross beta activity of 20.04 ± 1.93 and 23.47 ± 1.91 Bq/Kg respectively. The gross alpha activity concentrations for the soils locations were 8.82 ± 3.38

Table 1. Gross alpha and beta activity concentrations in leaf, stem and soil samples.

S/N	Sample ID	Sample type	Alpha activity (Bq/kg)	Beta activity (Bq/kg)
1.	UL1	Leaf	3.55±2.05	80.32±2.25
2.	UL2	Leaf	13.95±4.03	12.67±1.82
3.	US1	Stem	3.61 ± 2.08	20.04±1.93
4.	US2	Stem	3.53 ± 2.04	23.47±1.91
5.	SOI 1	Soil	8.82 ± 3.38	196.30±2.98
6.	SOI 2	Soil	10.15±3.54	87.11 ± 2.04

Table 2. Gross alpha and beta radioactivity concentrations for cassava samples.

S/N	Gross alpha and beta radioactivity concentrations			
	Sample ID	Sample type	Alpha activity (Bq/kg)	Beta activity (Bq/kg)
1	A1F	Cassava	0.39 ± 0.02	0.65 ± 2.66
2	A1S	Soil	0.37 ± 0.01	0.69 ± 2.84
3	A2F	Cassava	0.07 ± 0.02	0.43 ± 2.70
4	A2S	Soil	0.53 ± 0.02	0.46 ± 2.71
5	A3F	Cassava	0.28 ± 0.01	0.63 ± 2.83
6	A3S	Soil	0.45 ± 0.02	0.53 ± 2.54
7	A4F	Cassava	0.60 ± 0.02	0.89 ± 2.60
8	A4S	Soil	0.35 ± 0.02	1.04 ± 2.35

and 10.15 ± 3.54 Bq/Kg for locations 1 and 2 respectively while the gross beta activity concentrations were 196.30 ± 2.98 and 87.11 ± 2.04 Bq/Kg for the locations 1 and 2, respectively.

A higher gross alpha activity concentrations were recorded for the leaves of the fluted pumpkin than the stems, while that of the gross beta activity concentrations varies. The gross alpha activity from the old coal mine area was quite lower than that obtained for vegetables in old Uranium mine site in Udaipur, Rajasthan (Pathak and Pathak, 2012).

The results for the gross alpha and beta activity concentrations in cassava crop and their constituent soils are presented in Table 2. The gross alpha activity concentrations for cassava and soil samples ranged from 0.07 to 0.60 Bq/Kg and 0.35 to 0.53 Bq/Kg, respectively while the gross beta activity concentrations ranged from 0.43 to 0.89 Bq/Kg and 0.46 to 1.04 Bq/Kg for the cassava and soil samples, respectively.

Generally, the ranges of the beta activity concentrations were observed to be higher than that of the alpha activity concentrations. The results obtained in this study were slightly low when compared with the mean gross alpha and beta activity concentration reported by Jibiri and Fasae (2013), which reported that the gross beta activity concentration for farm soils from the northern part of Nigeria varied from 360.0 to 570.0 Bq/kg while for the alpha activities it varied from 8.0 to 40.0 Bq/kg. Also, the results obtained from this work are slightly lower when compared to the work done by

Ogundare and Adekoya (2015). They reported that the mean gross alpha and beta activities in soil samples were between 32.0 and 64.0 Bq/kg and 411.5 and 2710.0 Bq/kg, respectively. The mean gross alpha activities is much lower than those of selected oil fields around Imirigin, Bayelsa state and Rivers State (Anekwe et al., 2013; Meindinyo and Agbalagba, 2012).

Conclusion

The gross alpha and beta activity concentrations in cassava, fluted pumpkin and soils samples have been determined using alpha/beta spectroscopy. The result of this study showed that the Iva-valley coal mine area has lower gross alpha and beta activity concentrations compared to other areas of the country. This shows that the coal mining activities in the area may not have increased the radiation burden of the area.

CONFLICT OF INTERESTS

The authors have not declared any conflict of interests.

REFERENCES

Addo MA, Darko EO, Gordon C, Nyarko BJB (2013). A preliminary study of natural radioactivity ingestion from cassava grown and consumed by inhabitants around a cement production facility in the

Volta region , Ghana. International Journal of Environmental Sciences 3(6):2312-2323.

Amakom CM, Jibiri NN, Orji CE (2015). Gross alpha and beta activity concentrations in cassava tubers (*Manihot esculenta*) from old coal mining Area in Enugu, South Eastern Nigeria. British Journal of Applied Science and Technology, 9(2):200-205.

Akpa TC, Mallam SP, Ibeanu IG, Onoja RA (2004). Characteristics of Gross Alpha/Beta Proportional Counter. Nigerian of Journal of Physics, 16(1):13-18.

Anekwe UL, Avwiri GO, Agbalagba EO (2013). Assessment of Gamma-Radiation Levels in Selected Oil Spilled Areas in Rivers State, Nigeria. Energy science and Technology 285(1):33-37.

Farai IP, Jibiri NN (2000). Baseline studies of terrestrial outdoor gamma dose rate levels in Nigeria. Radiation Protection Dosimetry, 88(3):247-254.

Jibiri NN, Bankole OS (2006). Soil radioactivity and radiation absorbed dose rates at roadsides in high-traffic density areas in Ibadan metropolis, southwestern Nigeria. Radiation protection dosimetry 118(4):453-458.

Jibiri NN (2001). Assessment of health risk levels associated with terrestrial gamma radiation dose rates in Nigeria. Environment International, 27(1):21-26.

Jibiri NN, Fasae KP (2012). Activity concentrations of 226Ra, 232Th and 40K in brands of fertilisers used in Nigeria. Radiation Protection Dosimetry 148(1):132-137.

Jibiri NN, Fasae KP (2013). Gross alpha and beta activities and trace heavy elemental concentration levels in chemical fertilizers and agricultural farm soils in Nigeria. Natural Science, 9-5(01):71.

Ogundare FO, Adekoya OI (2015). Gross alpha and beta radioactivity in surface soil and drinkable water around a steel processing facility. Journal of Radiation Research and Applied Sciences 8(3):411-417.

Meindinyo RK, Agbalagba EO (2012). Radioactivity concentration and heavy metal assessment of soil and water, in and around Imirigin oil field, Bayelsa state, Nigeria. Journal of environmental chemistry and Ecotoxicology, 22-4(2):29-34.

Pathak B, Pathak A (2012). Estimation of gross alpha activity in soil and plant samples in Udaipur, Rajasthan. International Journal of Scientific and Engineering Research, 3(6).

Shanthi G, Maniyan CG, Raj GA, Kumaran JT (2009). Radioactivity in food crops from high-background radiation area in southwest India. Current Science, 10:1331-1335.

AJ ACADEMIC JOURNALS
expand your knowledge

International Journal of Physical Sciences

Full Length Research Paper

Effect of annealing temperature on the optical properties of Sb-ZnO thin films prepared using co-sputtering technique

Hend Alkhammash

Department of Physics, Faculty of Sciences, Taif University, Taif 888, Saudi Arabia.

Transparent conducting oxide thin films of Sb-ZnO were prepared on optically flat quartz by radio-frequency (RF) sputtering method. The scan electron microscope was used to characterize the topological morphology of the surface of the as-prepared and annealed films at (300, 400, 470, and 525°C) for 4 h in air. The optical properties of the films were deliberated using their reflectance and transmittance spectra at normal incident light. The optical energy band gap energy (Eop) values were found to increase by elevating the annealing temperatures. The dispersion curves of the refractive index of Sb-ZnOthin films were found to follow the single oscillator model. Optical parameters such as refractive index, real and imaginary parts of the dielectric constant, and optical conductivity were investigated.

Key word: Sputtering, thin film, Sb-ZnO, optical gap, refractive index.

INTRODUCTION

Zinc oxide is an auspicious material for optoelectronic devices due to its big band gap (3.37 eV). The n-type zinc oxide materials can be acquired by doping with Aluminum, Gallium or Indium. Besides, p-type ZnO considered to be low resistivity and high mobility it is hard to be fabricated with good quality, where, it is related to the construction of native donor defects such as Oxygen vacancies and Zinc interstitials (Look et al., 1999). The most used acceptor dopants for p-type zinc oxide is antimony Sb, nitrogen, and phosphorous (Minegishi et al., 1997; Lu et al., 2004; Joseph et al., 1999; Chen et al., 2005; Limpijumnong et al., 2005; Zhao et al., 2003). Doping ZnO with Sb was supposed to substitute Zn atom

(Limpijumnong et al., (2004). Xiu et al. (2005) have carried out p-type ZnO:Sb film by molecular beam epitaxy and pulsed laser deposition (Xiu et al., 2005; Pan et al., 2007; Zi-Wen et al., 2010; Liang et al., 2015) confirming that Sb is a promising dopant for realizing p-type zinc oxide. Doping zinc oxide with tin oxide reveal that, increasing the content of tin oxide, ZnO nanocrystal changed from near spherical to dumbbell-like (Duan et al., 2017). Thermal annealing processing is used to enhance the properties of semiconductor material. Electro-deposition of Sb_2S_3 absorber on TiO_2 nanorod array as photocatalyst for water oxidation has been investigated (Hong et al., 2018). As far as the author

E-mail: drhalkhammash@gmail.com, khamash.h@tu.edu.sa.

know, the effects of thermal annealing on Sb-doped ZnO thin films are rarely reported. So, this work focused on the effect of thermal annealing on the optical properties of Sb-ZnO.

EXPERIMENTAL TECHNIQUE

Thin films of Sb-ZnO were deposited on pre cleaned quartz substrates using sputtering unit model UNIVEX 350.The targets of ZnO and Sb are from Cathay Advanced Materials Limited Company. The base pressure of about 10^{-6} torr and sputtering pressure of about 2×10^{-2} torr. The distance between the substrate and target was 10 cm with an angle 65°. The standers cubic centimeter per minute (sccm) was kept constant at 20 cm^3/min with rotation of substrate 2 rpm. The power on ZnO and Sb targets was kept constant of 100 W and 20 W respectively. The rate of deposition was kept at 2 nm/min. The thickness of the films were determined using multiple-beam Fizeau fringes in reflection (Tolansky, 1949). The scanning electron microscope (SEM) (Hitachi S4700) was used for characterizing the surfaces of the films. The double beam spectrophotometer (JASCO model V-670 UV–Vis–NIR) was used for detecting the transmittance T(λ) and reflectance at R(λ) at nearly normal incidence in the range of wavelength 300 to 1800 nm. The absolute values of T(λ) and R(λ) are given by El-Nahass (1992).

$$T = (\frac{I_{ft}}{I_g})(1-R_g)$$

(1)

since I_{ft} is the light intensity passing through the film and substrate, I_g is the light intensity passing through the reference, and R_g is the substrate reflectance, and the reflectance R is as follows:

$$R = (\frac{I_{fr}}{I_m})R_m(1+[1+R_g]^2)-T^2R_g$$

(2)

I_m is the light intensity reflected from the reference mirror, I_{fr} is the light intensity reflected from the sample and R_m is the reflectance of the mirror.

In order to estimate the optical energy gap in the absorption region of the spectra, the absorption coefficient α and the absorption index, K, of the films at different wavelengths can be calculated using the following equations (Giulio et al., 1993; El-Nahass et al., 2010a, b):

$$\alpha = \frac{1}{t}Ln[\frac{(1-R)^2}{2T}+\sqrt{\frac{(1-R)^4}{4T^2}+R^2}],$$

(3)

$$K = \frac{\alpha\lambda}{4\pi},$$

(4)

where t is the film thickness.

RESULTS AND DISCUSSION

As shown in Figure 1a, the scan electron micrograph of the as-deposited film contain big grains besides, the films

annealed at 400 and 525°C show more tighter crystal grains and the grain volume became smaller as shown in Figure 1b, c. This change in grain size is due to annealing which gaining the atoms of the thin films extra energy, and enhance crystallinity of the films; also, annealing can activate the Sb-as an acceptor (Zhao et al., 2011).

The transmittance spectra of Sb-ZnO thin films are shown in Figure 2 which reveal an excellent surface quality and homogeneity of the films due to the appearance of interference fringes (Abd El-Raheem et al., 2009). It is observed that, sharp interference fringes appeared and indicated that the air/layer and layer/glass interfaces are flat and parallel (El-Nahass et al., (2010b). Figure 2 shows also that the transmittance increased with elevating the annealing temperature, this is attributed to the decrease of the size of the particle.

The optical energy E_{op} was depicted from Figure 3 representing the plots of $(\alpha h\nu)^2$ versus ($h\nu$) revealing that the direct optical gap widened with elevating the annealing temperature, this may be due to atomic rearrangement during the annealing process. Therefore, some defects will be removed leading to minimizing the density of dangling bonds causing the widening of optical gap (Mansour et al., 2010). Another interpretation of this widening may be due to an enhancement in the crystalline structure of the film, since, if the film becomes more polycrystalline, a decrease in the band gap defects leading to band gap band gap broadening (Atta et al., 2016). Using Swanepoel, (1983, 1984) and Manifacier et al. (1976) methods, the refractive index of refraction n can be calculated. The index of refractive n of the thin films can be calculated using the equations:

$$n = \sqrt{N + \sqrt{N^2 + s^2}}$$

(5)

$$N = \frac{1+s^2}{2} + \frac{2s(T_M - T_m)}{T_M T_m}$$

(6)

$$s = \frac{1}{T_s} + \sqrt{\frac{1}{T_s}-1}$$

(7)

where T_s is the substrate transmission, T_M the maximum of the transmittance curves, T_m is the identical minimum determined at the same wavelength λ.

Figure 4 displays the refractive index spectra for the Sb-ZnO films suggesting normal dispersion behavior. Furthermore, n decreases with raising the annealing temperature according to increasing the transparency of the films with increasing annealing temperature (Mohamed et al., 2006), which is affirmed by our results.

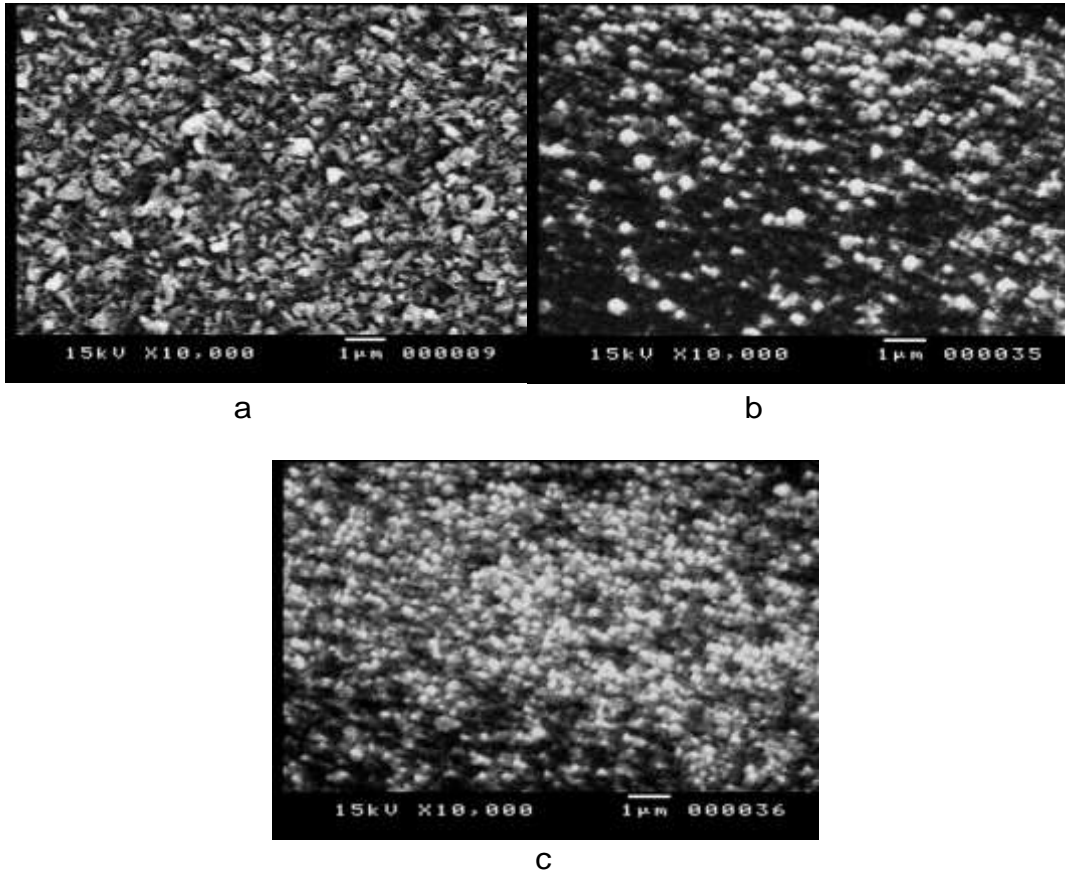a   b

c

Figure 1. Scan electro micrograph for Sb-ZnO thin films a- as deposited, b- annealed at 400°C, and c- at 525°C respectively.
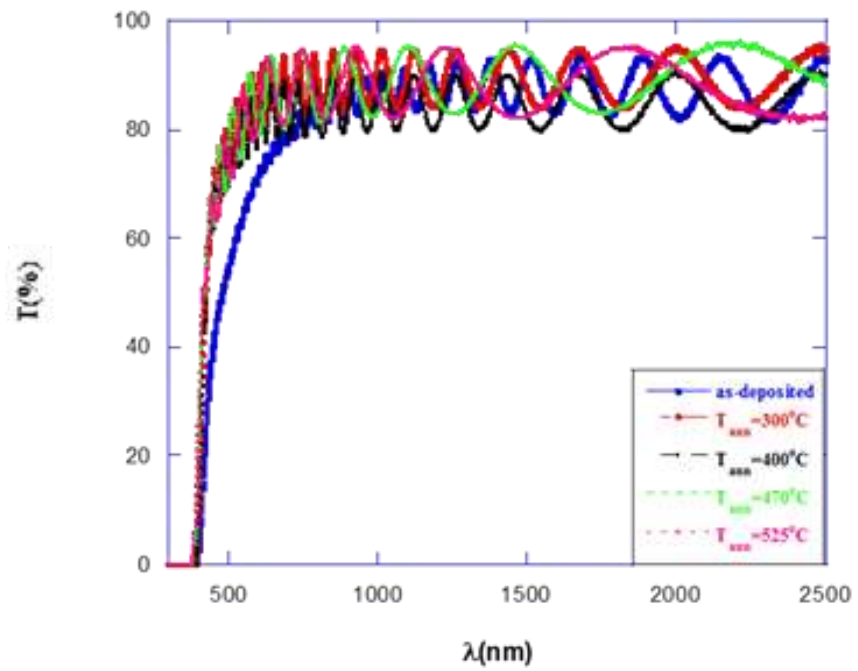
Figure 2. Tranmittance spectra for a deposited and annealed Sb-ZnO thin films at different temperatures.
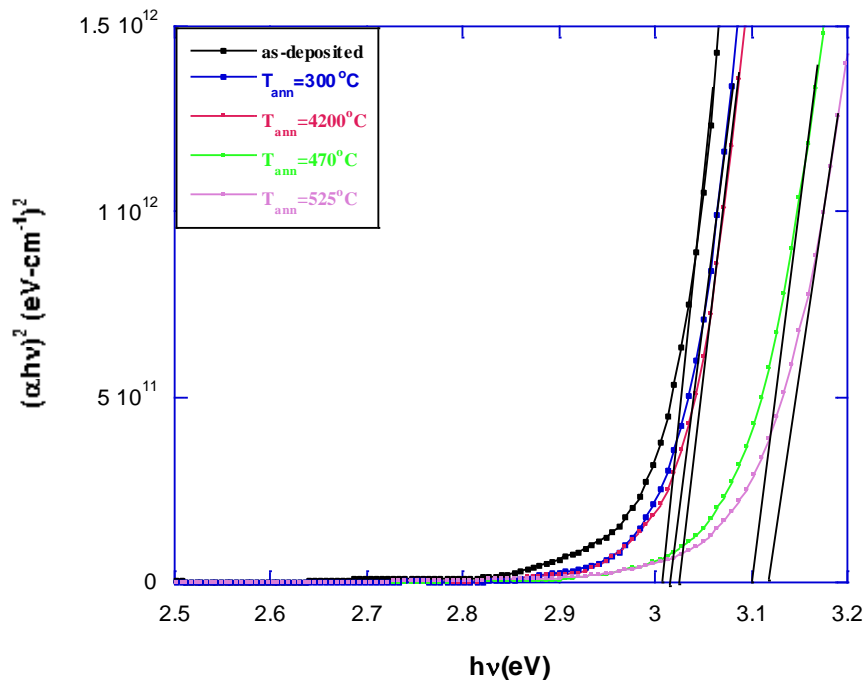
Figure 3. Plots of $(\alpha h\nu)^2$ vesus photon energy for Sb-ZnO thin films annealed at different temperatures.
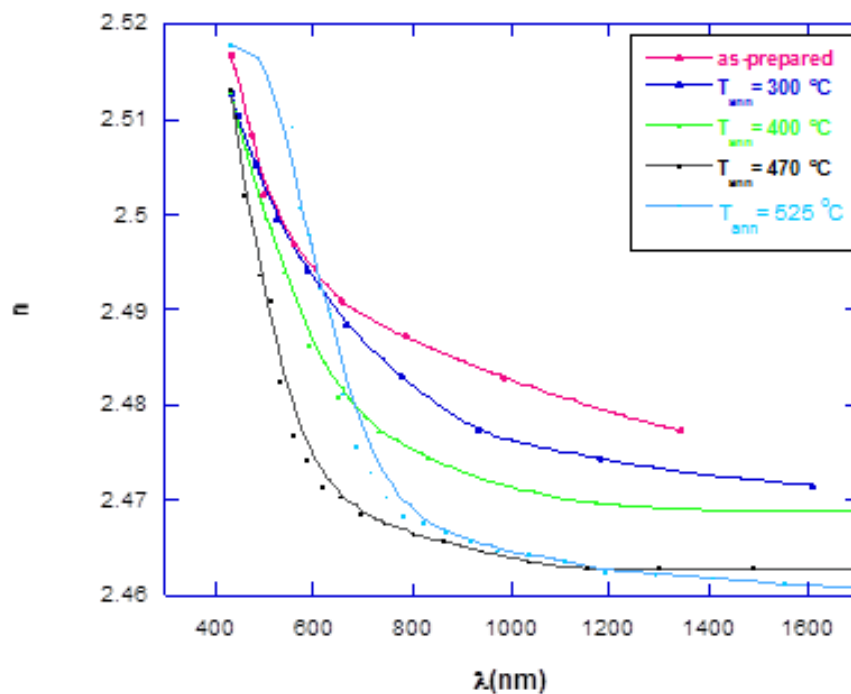
Figure 4. Spectra of the refractive index for as-prepared and annealed Sb-ZnO thin films.

The dielectric function ε is characterized as $\varepsilon = \varepsilon_1 + i\varepsilon_2$, the real part $\varepsilon_1 = n^2 - k^2$, the imaginary part $\varepsilon_2 = 2nk$ is of the dielectric constant representing the dispersion and absorption respectively. $\tan\delta$ represents the loss
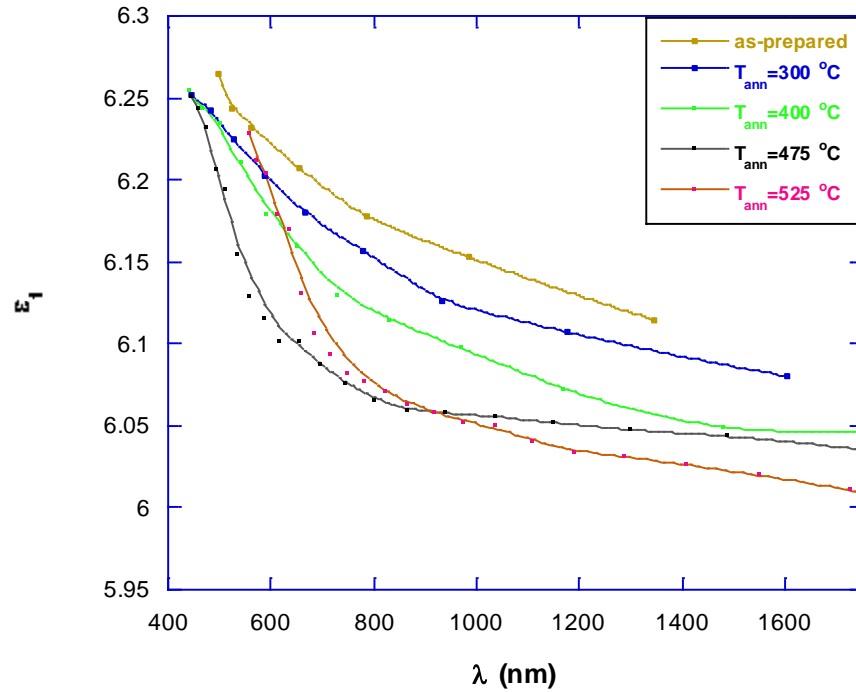
Figure 5. Spectra of the real part of the dielectric constant for as prepared and annealed Sb-ZnO thin films.
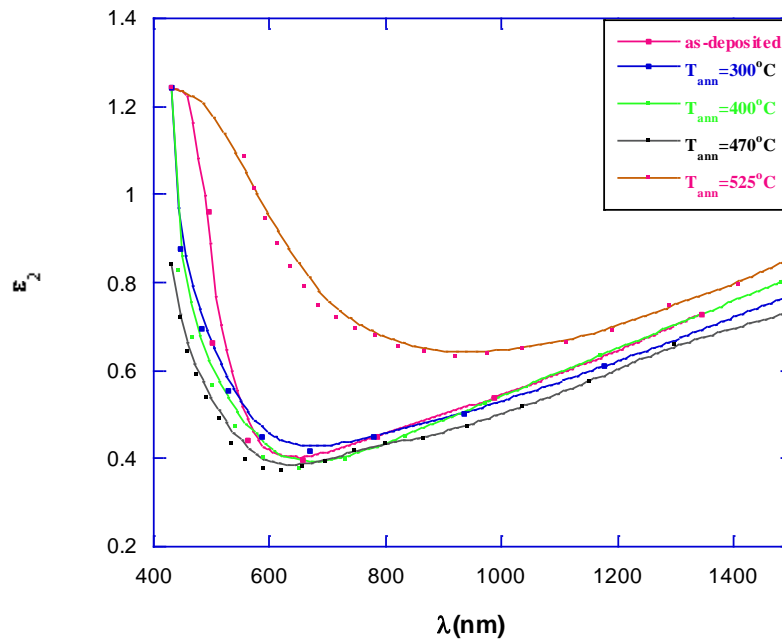
Figure 6. Spectra of imaginary part of the dielectric constant for as-deposited and annealed Sb-ZnO thin films at different temperatures.

factor. The dispersion and absorption spectra for antimony doped zinc oxide thin films prepared under different annealing temperatures are inspected in Figures 5 and 6 respectively. It is evident that ε_1 behaves as the n as seen in Figure 5 ε_2 fundamentally shows a decrease with wavelength and then increase with prolongating the
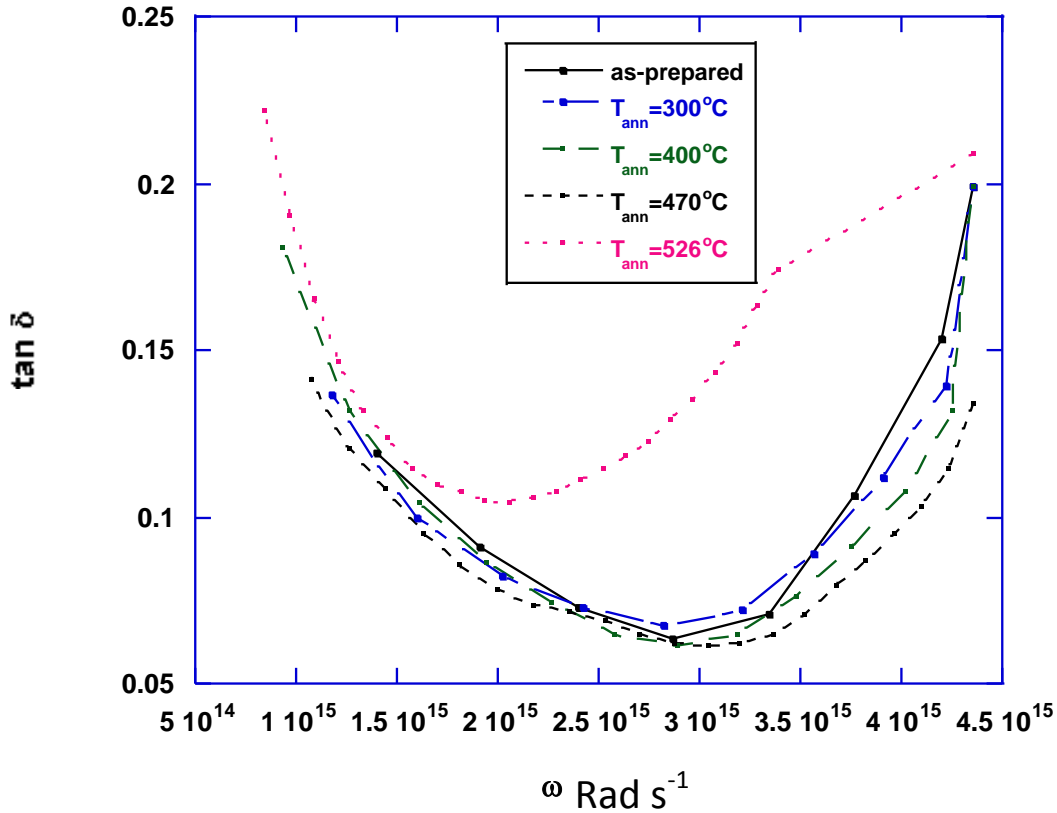
Figure 7. Variations of tan δ with changing the angular frequency for as-prepared and annealed Sb-ZnO thin films.

wave length depending on the annealing temperature as displayed in Figure 6 which is linked to the variation of absorption α with photon wavelength.

The changes of tanδ with angular frequency ω equal ($\omega = 2\pi f$ since f is the frequency) is drawn in Figure 7. The latter figure reveal that dissipation factor behaves as the loss factor more or less. The real and imaginary component σ_1 and σ_2 of optical conductivity are represented as (El-Nahass et al., 2014):

$$\sigma_1 = \omega\varepsilon_o\varepsilon_2, \qquad \sigma_2 = \omega\varepsilon_o\varepsilon_1$$

where the permittivity of frees pace is ε_o. The spectra of σ_1 are shown in Figure 8. It can be seen that σ_1 increases by increasing photon energy as shown in Figure 8 which can be owed to the excitation of the electrons by photon energy (Shaaban et al., 2006).

The surface and volume energy loss functions (SELF and VELF) can be calculated by using the relations (El-Nahass et al., 2014):

$$VELF = \frac{\varepsilon_2^2}{\varepsilon_1^2 - \varepsilon_2^2}$$

(8)

$$SELF = \frac{\varepsilon_2^2}{(\varepsilon_1 + 1)^2 + \varepsilon_2^2}$$

(9)

As seen in Figure 9 the VELF decrease with raising the photon energy at low range of energy and then increases with raising the energy of the photon e. Furthermore, Figure 10 indicate that SELF behaves as VELF. Using the theory of Wemple and DiDomenico (1971), the dispersion energy E_d and the single oscillator energy E_o can be calculated using the following formula:

$$\frac{1}{(n^2-1)} = \frac{E_0}{E_d} - \frac{1}{E_oE_d}(h\nu)^2$$

(10)

Since, (hv) is the incident photon energy.

The dispersion and the single oscillator energies are obtained from the slope and intercept of the plot $(n^2 - 1)^{-1}$ versus $(hv)^2$ as seen in Figure 11 for the Sb-ZnO thin films. The values of E_d and E_o are 30.5, 68.4, 68.5, 70.9, 62.3 eV, and 29.3, 13.4, 13.6, 14.1, 12.4 eV for the as-prepared and annealed film at 300, 400, 475, and 525°C respectively. It is obvious that the dispersion has a tendency to increase with raising the annealing temperature, whereas the single oscillator energy has a
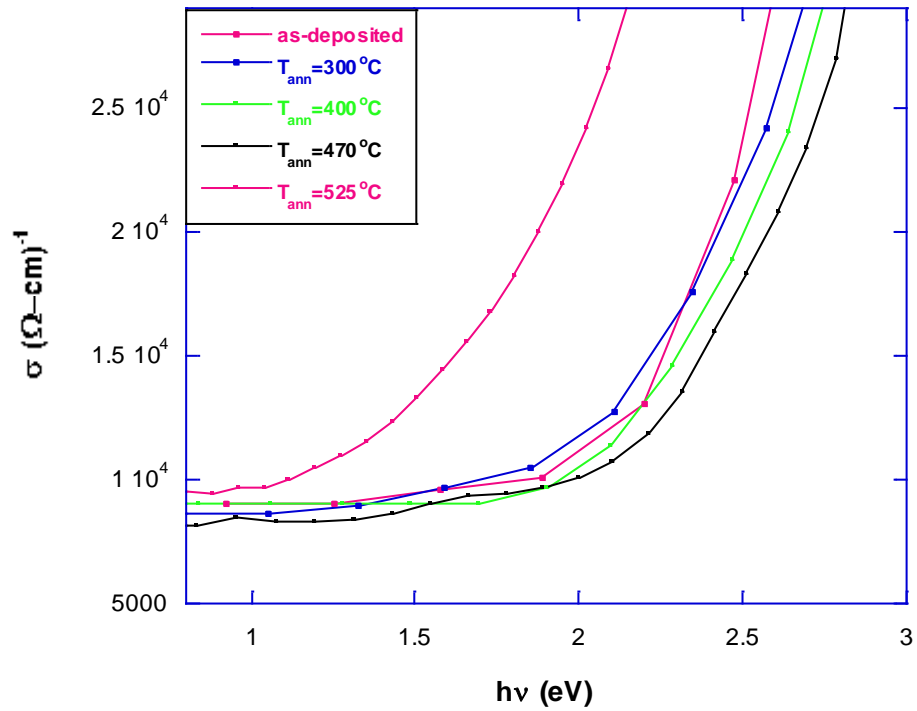
**Figure 8.** Variations of the optical conductivity with photon energy for as- deposited and annealed Sb-ZnO thin films at different temperetures.
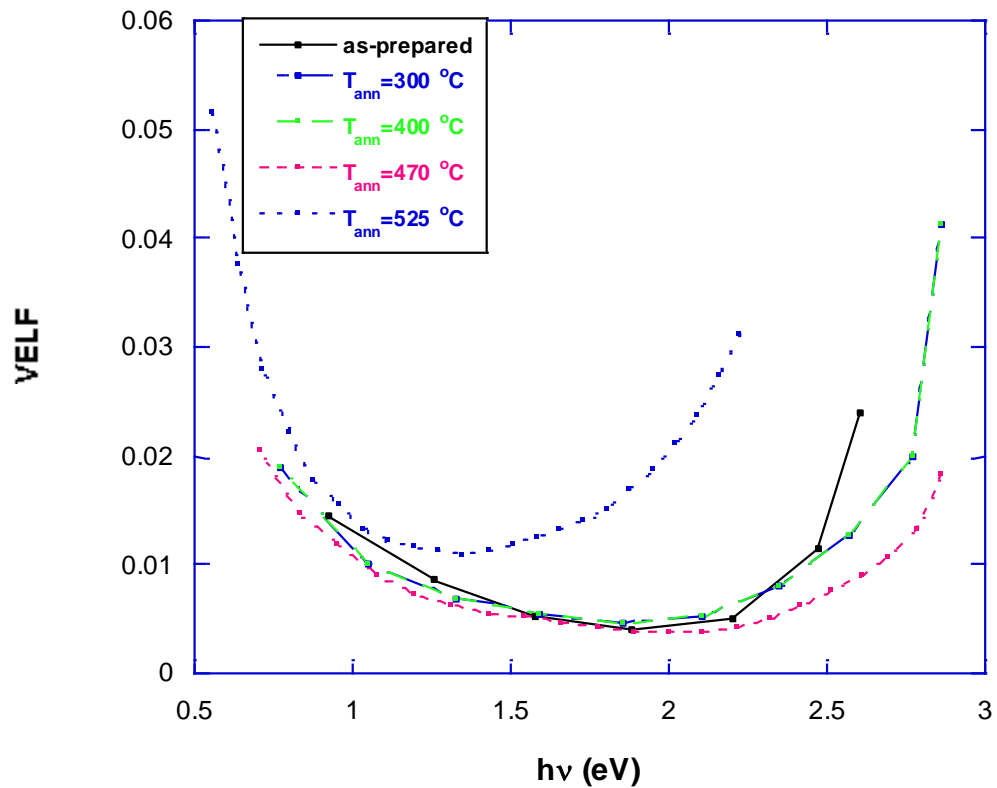
Figure 9. Variations of VELF with photon energy for as-prepared and annealed Sb-ZnO thin films.
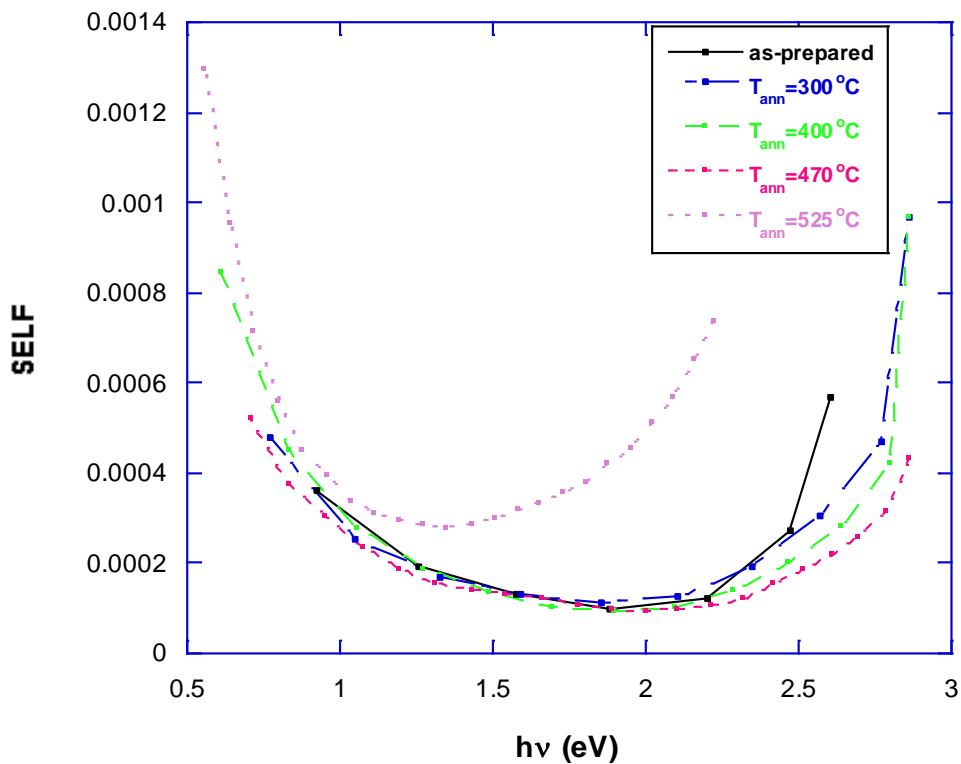
Figure 10. Variations of SELF with photon energy for as-prepared and annealed Sb-ZnO thin films.
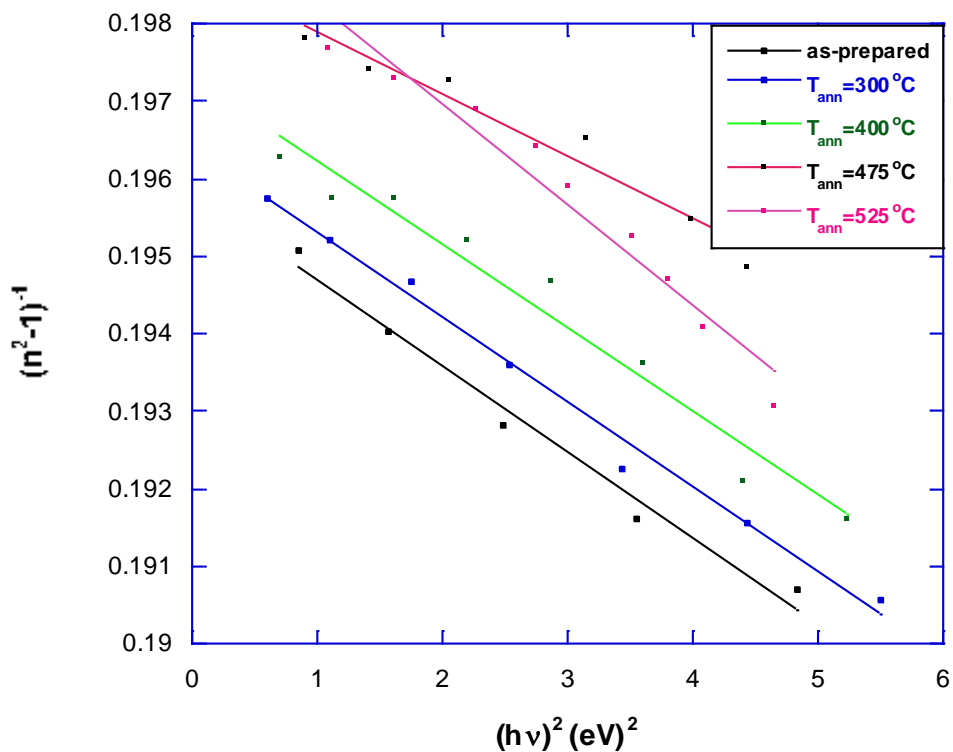
Figure 11. Variations of $(n^2-1)^{-1}$ with square of photon energy for as-prepared and annealed Sb-ZnO thin films.

tendency to lower with elevating the annealing temperature.

Conclusion

For preparing antimony doped zinc oxide thin films, the Co-sputtering technique was used. It was found that the optical gap increases with raising the annealing temperature. Normal dispersion describes the behavior of the refractive index, and optical conductivity increase with raising the incident photon energy. Dispersion energy has a tendency to increase with raising the annealing temperature, whereas single oscillator energy has a tendency to lower with raising annealing temperature. Surface and volume energy loss functions found to depend on photon energy.

CONFLICT OF INTERESTS

The author has not declared any conflict of interests.

REFERENCES

Abd El-Raheem MM, Ali HM, El-husainy NM (2009). Characterization of electron beam evaporated CdTe thin films for optoelectronic devices. Journal of Optoelectronics and Advanced Materials 11(6):813-819.

Atta AA, El-Nahhas MM, Elsabawy M, AbdEl-Raheem MM, Hasaanien AM, Alhuthali A, Merazga A (2016). Optical characteristics of transparent samarium oxide thin films deposited by the radio-frequency sputtering technique. Pramana 87(5):72.

Chen LL, Lu JG, Ye ZZ, Lin YM, Zhao BH, Ye YM, Zhu LP (2005). p -type behavior in In–N codoped ZnO thin films. Applied Physics Letters 87(25):252106.

Duan M, Wang J, Liu C, Xie J, Han J (2017). Effects of SnO doping on the optical properties of ZnO in glass. Journal of Non-Crystalline Solids 459:32-35.

El-Nahass MM (1992). Optical properties of tin diselenide films. Journal of Materials Science 27(24):6597–6604.

El-Nahass MM, Atta AA, Abd El-Raheem MM, Hassanien AM (2014). Structural and optical properties of DC Sputtered Cd2SnO4 nanocrystalline films. Journal of Alloys and Compounds 585:1-6.

El-Nahass MM, El-Deeb AF, Metwally HS, El-Sayed HEA, Hassanien AM (2010b). Influence of X-ray irradiation on the optical properties of iron (III) chloride tetraphenylporphyrin thin films. Solid State Sciences 12(4):552-557.

El-Nahass MM, El-Deeb AF, Metwally HS, Hassanien AM (2010a). Structural and optical properties of iron (III) chloride tetraphenylporphyrin thin films. The European Physical Journal Applied Physics 52(1):10403.

Giulio M Di, Micocci G, Rella R, Siciliano P, Tepore A (1993). Optical Absorption of Tellurium Suboxide Thin Films. Physica Status Solidi (a) 136(2):K101–K104.

Hong J-Y, Lin L-Y, Li X (2018). Electrodeposition of Sb2S3 light absorbers on TiO$_2$ nanorod array as photocatalyst for water oxidation. Thin Solid Films 651:124-130.

Joseph M, Tabata H, Kawai T (1999). p-Type Electrical Conduction in ZnO Thin Films by Ga and N Codoping. Japanese Journal of Applied Physics 38(Part 2,11A):L1205–L1207.

Liang H, Chen Y, Xia X, Feng Q, Liu Y, Shen R, Du G (2015). Influence of Sb valency on the conductivity type of Sb-doped ZnO. Thin Solid Films 589:199-202.

Limpijumnong S, Li X, Wei SH, Zhang SB (2005). Substitutional diatomic molecules NO, NC, CO, N2, and O2: Their vibrational frequencies and effects on p doping of ZnO. Applied Physics Letters 86(21):211910.

Limpijumnong S, Zhang SB, Wei SH, Park CH (2004). Doping by Large-Size-Mismatched Impurities: The Microscopic Origin of Arsenic- or Antimony-Doped p -Type Zinc Oxide. Physical Review Letters 92(15):155504.

Look DC, Hemsky JW, Sizelove JR (1999). Residual Native Shallow Donor in ZnO. Physical Review Letters, 82(12):2552-2555.

Lu J G, Ye ZZ, Zhuge F, Zeng YJ, Zhao BH, Zhu LP (2004). p-type conduction in N–Al co-doped ZnO thin films. Applied Physics Letters, 85(15):3134-3135.

Manifacier JC, Gasiot J, Fillard JP (1976). A simple method for the determination of the optical constants n, k and the thickness of a weakly absorbing thin film. Journal of Physics E: Scientific Instruments 9(11):1002-1004.

Mansour B, Shaban H, Gad S, El-Gendy Y, Salem MA (2010). Effect of Film Thickness, Annealing and Substrate Temperature on the Optical and Electrical Properties of CuGa0.25In0.75Se2 Amorphous Thin Films. Journal of Ovonic Research 6(1):13-22

Minegishi K, Koiwai Y, Kikuchi Y, Yano K, Kasuga M, Shimizu A (1997). Growth of p-type Zinc Oxide Films by Chemical Vapor Deposition. Japanese Journal of Applied Physics 36(Part 2, 11A):L1453–L1455.

Mohamed HA, Ali HM, Mohamed SH, Abd El-Raheem MM (2006). Transparent conducting ZnO-CdO thin films deposited by e-beam evaporation technique. The European Physical Journal Applied Physics, 34(1):7-12.

Pan X, Ye Z, Li J, Gu X, Zeng Y, He H, Zhu L, Che Y (2007). Fabrication of Sb-doped p-type ZnO thin films by pulsed laser deposition. Applied Surface Science, 253(11):5067-5069.

Shaaban ER, El-Kabnay N, Abou-sehly AM, Afify N (2006). Determination of the optical constants of thermally evaporated amorphous As40S60, As35S65 and As30S70 using transmission measurements. Physica B: Condensed Matter, 381(1-2):24-29.

Swanepoel R (1983). Determination of the thickness and optical constants of amorphous silicon. Journal of Physics E: Scientific Instruments 16(12):1214-1222.

Swanepoel R (1984). Determination of surface roughness and optical constants of inhomogeneous amorphous silicon films. Journal of Physics E: Scientific Instruments 17(10):896-903.

Tolansky S (1949). Multiple-Beam Interferometry Surface and Films, London: Oxford University Press.

Wemple SH, DiDomenico M (1971). Behavior of the Electronic Dielectric Constant in Covalent and Ionic Materials. Physical Review B 3(4):1338-1351.

Xiu FX, Yang Z, Mandalapu LJ, Zhao DT, Liu JL, Beyermann WP (2005). High-mobility Sb-doped p-type ZnO by molecular-beam epitaxy. Applied Physics Letters 87(15):152101.

Zhao B, Yang H, Du G, Miao G, Zhang Y, Gao Z, Fang X (2003). High-quality ZnO/GaN/Al2O3 heteroepitaxial structure grown by LP–MOCVD. Journal of Crystal Growth, 258(1-2):130-134.

Zhao Z, Hu L, Zhang H, Sun J, Bian J, Zhao J (2011). Effect of different annealing temperature on Sb-doped ZnO thin films prepared by pulsed laser deposition on sapphire substrates. Applied Surface Science 257(11):5121-5124.

Zi-Wen Z, Li-Zhong H, He-Qiu Z, Jing-Chang S, Ji-Ming B, Kai-Tong S, Xi C, Jian-Ze Z, Xue L, Jin-Xia Z (2010). Effect of Different Substrate Temperature on Sb-Doped ZnO Thin Films Prepared by Pulsed Laser Deposition on Sapphire Substrates. Chinese Physics Letters 27(1):017301.

Related Journals:

African Journal of
Pure and Applied Chemistry

Journal of
Environmental Chemistry
and Ecotoxicology

Journal of
Geology and Mining Research

Journal of
Internet and
Information Systems

Journal of
Oceanography and
Marine Science

Journal of
Petroleum Technology
and Alternative Fuels

Journal of
Agricultural
Biotechnology and
Sustainable Development

International Journal of
Physical Sciences

Scientific Research and Essays